Effect of annealing on mechanical properties of a nanocrystalline CoCrFeNiMn high-entropy alloy processed by high-pressure torsion

Hamed Shahmir, Junyang He, Zhaoping Lu, Megumi Kawasaki, Terence G. Langdon

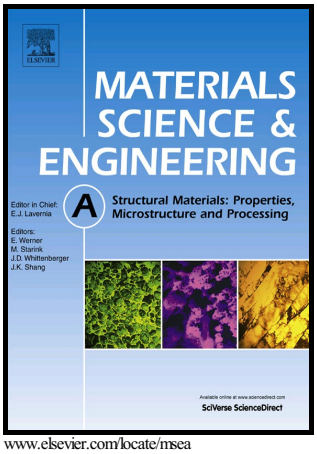

www.elsevier.com/locate/msea

PII: S0921-5093(16)31054-1
DOI: http://dx.doi.org/10.1016/j.msea.2016.08.118
Reference: MSA34076

To appear in: *Materials Science & Engineering A*

Received date: 22 July 2016
Revised date: 29 August 2016
Accepted date: 30 August 2016

Cite this article as: Hamed Shahmir, Junyang He, Zhaoping Lu, Megum Kawasaki and Terence G. Langdon, Effect of annealing on mechanical properties of a nanocrystalline CoCrFeNiMn high-entropy alloy processed by high-pressur torsion, *Materials Science & Engineering A* http://dx.doi.org/10.1016/j.msea.2016.08.118

Effect of annealing on mechanical properties of a nanocrystalline CoCrFeNiMn high-entropy alloy processed by high-pressure torsion

Hamed Shahmir[a,*], Junyang He[b], Zhaoping Lu[b], Megumi Kawasaki[c], Terence G. Langdon[a]

[a] Materials Research Group, Faculty of Engineering and the Environment, University of Southampton, Southampton SO17 1BJ, UK

[b] State Key Laboratory for Advanced Metals and Materials, University of Science and Technology Beijing, Beijing 10083, People's Republic of China

[c] Division of Materials Science and Engineering, Hanyang University, Seoul 133-791, South Korea

[*]Corresponding author. Tel.: +442380594438. H.Shahmir@soton.ac.uk

Abstract

A CoCrFeNiMn high-entropy alloy (HEA) was processed by high-pressure torsion (HPT) under 6.0 GPa pressure up to 10 turns at room temperature. It is shown that there is a gradual evolution in hardness with increasing numbers of turns but full homogeneity is not achieved even after 10 turns. Microhardness measurements reveal that the material reaches a saturation hardness value of ~4.41 GPa and in this condition the microstructure shows exceptional grain refinement with a grain size of ~10 nm. An ultimate strength value of ~1.75 GPa and an elongation to fracture of ~4% were obtained in a sample processed for 5 turns. The nanostructured HEA was subjected to post-deformation annealing (PDA) at 473-1173 K and it is shown that the hardness increases slightly to 773 K due to precipitation and then decreases up to 1173 K due to a combination of recrystallization, grain growth and a dissolution of the precipitates. The formation of brittle precipitates, especially σ-phase, at 873 and 973 K significantly reduces the ductility. Short-term annealing for 10 min at 1073 K prevents grain growth and leads to a combination of high strength and good ductility including an ultimate tensile strength of ~830 MPa and an elongation to failure of ~65%.

Keywords: CoCrFeNiMn; High-entropy alloy; High-pressure torsion; Nanostructured materials; Post deformation annealing; Severe plastic deformation.

1. Introduction

High-entropy alloys (HEAs) are a new class of materials containing five or more principal elements with each elemental concentration between 5 at.% and 35 at.% but producing a relatively simple structure based on solid solution phases [1,2]. In practice, there is an opportunity for achieving a combination of high solid solution strengthening and good ductility if the solid solution phase possesses a simple crystal structure such as a face-centred cubic (*fcc*) lattice having a large number of slip systems [3]. As an example, and one of the best studied such single-phase HEAs, there is the equiatomic CoCrFeNiMn alloy [2]. Even though the separate elements in this quinary system possess different crystal structures, the alloy crystallizes as a single-phase *fcc* solid solution [4]. Furthermore, the CoCrFeNiMn alloy generally exhibits outstanding ductility and fracture toughness properties even at liquid nitrogen temperature [5]. Nevertheless, it is reasonable to anticipate that grain refinement using severe plastic deformation (SPD) methods may lead to additional strengthening in this alloy.

High-pressure torsion (HPT) is a well-established SPD procedure for obtaining ultra-fine and even nanostructured grains in metals and alloys [6]. In HPT processing, a disk-shaped specimen is deformed by simple shear between two anvils where it is constrained under a high pressure and subjected to concurrent torsional straining. Generally, nanostructured metals and alloys processed by HPT exhibit high strength but their ductility is limited because they have both a low rate of strain hardening and a low strain rate sensitivity [7-9]. Accordingly, short post-deformation annealing (PDA) of nanostructured metals is often important for improving the ductility. However, annealing at excessively high temperatures leads to an acceleration in recovery and recrystallization and thereby reduces the hardness. Therefore, selecting an appropriate annealing condition may result in both good ductility and high strength in HPT-processed nanostructured materials [10].

There are very few reports describing the influence of HPT processing on HEAs [11-16] and no systematic investigations are currently available describing the mechanical behavior of HEAs prepared by HPT processing and then subjected to PDA. Accordingly, the present

research was initiated to evaluate the effect of PDA on the microstructural evolution and mechanical properties of a CoCrFeNiMn alloy with the objective of optimizing the annealing conditions to produce a unique combination of high strength and good ductility.

2. Experimental material and procedures

The experiments were conducted on an HEA with a nominal composition of $Co_{20}Cr_{20}Fe_{20}Ni_{20}Mn_{20}$ (in at.%). The master alloy was prepared by arc-melting a mixture of pure metals (purity >99 wt.%) and the ingot was remelted at least four times to promote chemical homogeneity. The melted alloy was drop-cast into a mould to give a bar about 10×10 mm^2 with a length of ~60 mm. The as-cast alloy was homogenized at 1273 K for 16 h under an Ar-controlled atmosphere. Disks of 10 mm in diameter were prepared with electro-discharge machining to thicknesses of ~1 mm and they were then polished mechanically to final thicknesses of ~0.8 mm. These disks were processed by HPT at room temperature under quasi-constrained conditions [17] using an applied pressure, P, of 6.0 GPa and a rotation speed of 1 rpm through totals, N, of 1, 5 and 10 revolutions. The disks subjected to HPT through 5 rotations were used for PDA at 473-1173 K for total annealing times from 10 to 60 min.

After processing, each HPT disk was polished to a mirror-like quality and hardness measurements were taken using a Vickers microhardness tester with a load of 500 gf and dwell times of 10 s. The average microhardness values, Hv, were measured along randomly selected diameters on each disk. These measurements were taken at intervals of ~0.5 mm and at every point the local value of Hv was obtained from the average of four separate hardness values. The phase constituents were determined using X-ray diffraction (XRD) employing Cu Kα radiation (wavelength λ = 0.154 nm) at 45 kV and a tube current of 200 mA with Rigaku SmartLab equipment. The XRD measurements were performed over 2θ ranging from 30° to 100° using a scanning step of 0.01° and a scanning speed of 2° min^{-1}.

Microstructural characterizations were carried out using optical microscopy (OM),

scanning electron microscopy (SEM) and transmission electron microscopy (TEM). For the OM and SEM observations, the samples were ground through 800, 1200 and 4000 grit SiC papers, polished using a 40 nm colloidal silica suspension and then etched with a solution of 50 mL H_2O, 50 mL HCl and 10 g $CuSO_4$. Foils for TEM were prepared before and after PDA at 873 K for 60 min using a focused ion beam (FIB) Zeiss Nvision 40 FIB facility at 3 mm from the disk centres in the normal sections of the disks so that the normals of the images lay in the shear direction. The TEM micrographs were obtained using a JEOL JEM-3010 microscope operating under an accelerating voltage of 300 kV.

Two miniature tensile specimens with gauge dimensions of 1.1×1.0×0.6 mm^3 were cut from symmetric off-centre positions near the edges of each disk using electro-discharge machining. Similar tensile samples were also prepared from the initial cast HEA without HPT. Thus, the mechanical properties were examined in the HEA in the initial condition before HPT and after HPT processing followed by PDA at 773-973 K for 60 min and PDA at 1073-1173 K for periods of 10-60 min. Stress-strain curves were recorded using an initial strain rate of ~1.0 × 10^{-3} s^{-1} with a Zwick universal testing machine. Two samples were tested for each condition. The stress-strain curves were plotted for each specimen and the ultimate tensile strengths were derived directly from the curves. The elongations were estimated by carefully measuring the gauge lengths before and after tensile testing using an optical microscope.

3. Experimental results

3.1 Microstructure and hardness after HPT processing

The results for the Vickers microhardness measurements are shown in Fig. 1(a) after processing through different numbers of turns with the average values of Hv plotted along each disk diameter and with the lower dashed line at Hv ≈ 122 corresponding to the initial hardness in the homogenized condition. Inspection of Fig. 1(a) shows that, with reference to the homogenized condition, the hardness at the edge of the disk increases significantly by a factor

of ~3.7 to Hv ≈ 450 after only 1 turn whereas the hardness in the centre increases only to Hv ≈ 300. At the edges of the disks there is essentially an insignificant increase in hardness to Hv ≈ 455 through 5 and 10 turns whereas in the centre the hardness values gradually increase to Hv ≈ 380 after 10 turns. These results confirm the evolution in hardness with increasing torsional straining and the presence of a saturation hardness at Hv ≈ 455. However, even after 10 turns it was not possible to produce a fully-homogeneous hardness distribution and instead the results show that after 5 and 10 turns the area within a radius of $r < 1$ mm at the centres of the disks continues to have lower values of hardness. The results demonstrate also there is no significant difference between the hardness of samples processed through 5 and 10 turns at radii larger than ~1 mm. The variation of Hv with equivalent strain is shown in Fig. 1(b) for HEA disks processed through up to 10 turns and this plot confirms that the datum points reach a saturation hardness after an equivalent strain of ~20.

Figure 2 shows the XRD patterns for the initial homogenized sample (designated as $N = 0$) and near the edges of disks after HPT through 1 and 5 turns. It is apparent that the initial and HPT-processed microstructures consist of a single *fcc* phase and the HPT processing causes peak broadening in the HEA. It is important to note that there is no evidence for creating a new phase and the occurrence of the phase transformation during HPT processing.

The microstructures of the HEA are shown in Fig. 3 (a) initially and (b) after 5 turns of HPT for positions about 3 mm from the disk centres. The microstructure before HPT processing is typical of a fully-annealed sample consisting of equiaxed grains with sizes of ~100 μm. Some particles are also present in the homogenized condition as marked by white arrows in Fig. 3(a). Energy dispersive X-ray spectroscopy (EDS) was performed on these particles and showed oxygen, chromium and manganese peaks which indicates the presence of Cr-Mn oxides. These particles are inclusions that were reported previously in this alloy [18-20]. Figure 3(b) taken after 5 turns of HPT demonstrates that the processed microstructure consists of an array of equiaxed nanostructured grains having an average size of ~10 nm and with many of the grains

surrounded by diffuse or ill-defined grain boundaries. In addition, strain contrast is visible in many of these nano-scale grains which is associated with the presence of dislocations. The appearance of this microstructure is typical of materials prepared using SPD techniques and it is consistent with the presence of a large volume of high-energy non-equilibrium boundaries [21]. The arrangement of the diffraction spots in semi-continuous circles in the selected area electron diffraction (SAED) pattern confirms that the microstructure contains boundaries having high angles of misorientation. Some grains also contain nano-twins having a width of only a few nanometers, as shown by the yellow arrows in Fig. 3(b).

3.2 Microstructure and hardness after post-deformation annealing

Figure 4(a) shows the measured values of the microhardness for the homogenized sample without processing and the HPT-processed samples after annealing at temperatures of 473 to 1173 K for a period of 60 min. The results demonstrate that the hardness of the nanocrystalline HEA increases slightly up to Hv ≈ 530 after annealing at 773 K and then decreases rapidly with increasing annealing temperatures up to 1173 K. At this latter temperature, the hardness is very close to the value for the homogenized condition. It is interesting to note that the homogenized alloy also shows a similar trend but a maximum hardness in the coarse-grained material of only Hv ≈ 200. This behavior suggests that precipitates form at temperatures up to 773 K. All of the microhardness results after HPT followed by PDA at different temperatures for 60 min are summarized in Table 1. It should be noted that the grain size estimated though the XRD analysis refers to the crystallite size which is considered equivalent to the grain size especially when the microstructure is refined to the nano-scale [22].

Figure 4(b) shows results for Vickers microhardness measurements near the edges of the disks after HPT through 5 turns followed by PDA for 10 to 60 min at temperatures from 473 to 1173 K. These results confirm that the hardness of samples annealed for 60 min at 473-873 K remains higher than in the sample processed by HPT without annealing. In addition, there is an

insignificant change in hardness when the annealing time is increased from 10 to 60 min in this temperature range. The hardness of the HPT-processed sample drops after annealing at 973-1173 K for 10 min and the amount of this reduction is significant at 1173 K. Furthermore, increasing the annealing time at these temperatures leads to a gradual decrease in hardness.

Microstructural evaluations of the nanostructured HEA after PDA were conducted by XRD and the results are presented in Fig. 5. Inspection shows that several new peaks appear after annealing at temperatures from 473 to 1073 K and these peaks are of two different forms. First, the new peaks marked with open circles with the main peak at $2\theta \approx 44.2°$ are related to the formation of a new *bcc* phase which is precipitated within the *fcc*-phase matrix. According to the present results, the lattice parameter of this *bcc* phase is $a \approx 2.88$ Å which is in good agreement with the Cr-rich phase reported earlier in this HEA [12]. Second, close inspection of Fig. 5 reveals the appearance of some additional peaks of very low intensities marked with open squares in the samples annealed at 873 and 973 K. The crystal structure of this new phase was identified as tetragonal with lattice parameters of $a \approx 8.8$ Å and $c \approx 4.5$ Å where this is consistent with the σ-phase which is a hard Cr-rich phase reported earlier in HEAs [19,20,23,24].

Nevertheless, the XRD results in Fig. 5 indicate that the microstructure is again single phase after annealing at 1173 K. It should be noted that a similar trend was also observed after annealing the homogenized HEA without HPT processing except only that the σ-phase was not detected for this condition. The volume fractions of the precipitated phases and the grain sizes after HPT followed by PDA estimated from the XRD results are summarized in Table 1. The grain size of the HPT-processed sample estimated from XRD is consistent with TEM observations from Fig. 3(b). The results in Table 1 show that the volume fractions of precipitates decrease with increasing annealing temperature and finally approach zero at 1173 K. The highest volume fraction of precipitates was ~20% which was recorded at an annealing

temperature of 673 K.

A set of representative TEM images and appropriate SAED patterns are shown in Fig. 6 for the sample after HPT for 5 turns followed by PDA at 873 K for 60 min. Thus, in Fig. 6(a) the microstructure contains equiaxed grains in the range of ~40-120 nm with an estimated mean grain size of ~90 nm. The EDS results of the two regions marked by *A* and *B* in Fig. 6(b) confirmed from the chemical compositions that these neighbouring grains were different phases. Thus, the chemical composition of region *A* corresponded to the Cr-rich phase and the composition of region *B* corresponded to the composition of the HEA matrix. This analysis shows that the Cr-rich phase formed during PDA is distributed within the HEA matrix and has a similar grain size. Furthermore, a comparison between TEM images after HPT (Fig. 3(b)) and after PDA at 873 K for 60 min (Fig. 6(d)) shows that the grain boundaries after PDA are distinguished by a spreading of the thickness extinction contours which are a recognized feature of non-equilibrium grain boundaries [25]. Twins are also revealed in some bright grains as shown by arrows in Fig. 6 (b) and (d).

The formation of nano-scale precipitates within the primary matrix grains, as shown by the arrows in Fig. 6(b), is evident after HPT followed by PDA and an appropriate SAED pattern and EDS analysis of the grain including these nano-precipitates is shown in Fig. 6(c). New spots corresponding to the new *fcc* and *bcc* phases and the σ-phase are present in the SAED pattern but, for greater clarity, one-half of the SAED pattern before (left) and one-half after PDA at 873 K (right) are shown placed in adjacent positions in Fig. 7. In this combined format, it is readily apparent that there is a pronounced change in the diffraction patterns from continuous to discontinuous rings after conducting PDA. Thus, the yellow rings determine the *fcc* planes which are related to the matrix and the new sets of spots are clearly revealed after PDA. These results confirm the occurrence of a phase decomposition during PDA with one set of new spots corresponding to the *bcc*-phase in good agreement with the XRD results and the other new spots corresponding to the *fcc*-phase formed during PDA. It has been suggested that

this second *fcc*-phase, which is located mainly between the $(111)_{fcc}$ and $(200)_{fcc}$ rings, is related to the MnNi(Cr,Fe,Co) phase which corresponds to nano-scale precipitates forming during short-term annealing after SPD [12]. In addition, some weak sets of spots observed in the SAED pattern are in good correlation with the tetragonal σ-phase which was also detected by XRD.

Figure 8 shows representative microstructures of the HEA after HPT followed by PDA at 973 K in (a) SEM and (b) OM and also in OM after PDA for 60 min at (c) 1073 K and (d) 1173 K where these samples show a lower hardness compared with immediately after HPT as demonstrated in Fig. 4(b). All of these microstructures are equiaxed with average grain sizes of ~0.4, ~4 and ~17 μm after PDA at 973, 1073 and 1173 K, respectively, and these values are documented in Table 1. In addition, there is evidence for the existence of twins after PDA. The SEM micrograph of the sample annealed at 973 K in Fig. 8(a) shows the existence of the precipitated phase which, according to XRD results related to this annealing temperature and TEM observations of the sample annealed at 873 K, corresponds to precipitates of a Cr-rich phase. It is apparent that the Cr-rich phase is distributed homogenously in the microstructure in Fig. 8(b) with a grain size similar to that of the matrix in Fig. 8(a). It is also evident from Fig. 8(c) that recrystallization takes place during annealing at 1073 K giving an average grain size of ~4 μm. Finally, inspection of the microstructures after PDA at 1073 and 1173 K in Fig. 8(c) and (d) reveals almost no precipitates and this is consistent with the XRD results in Fig. 5.

3.3 Mechanical properties

Representative plots of engineering stress against engineering strain using an initial strain rate of 1.0×10^{-3} s^{-1} are shown in Fig. 9 for the homogenized specimen, an HPT sample processed through 5 turns and samples processed by HPT for 5 turns followed by PDA for 60 min at temperatures from 773 to 1173 K. Inspection of these curves shows that the initial un-processed sample exhibits the lowest flow stress but a large elongation to failure whereas HPT

processing gives a significant increase in strength but with a corresponding decrease in the measured elongation to failure. This trend is consistent with the classical mechanical behaviour of ultrafine-grained metals that are tested in tension at relatively low temperatures after processing using SPD techniques [26,27]. The results indicate that the ultimate tensile strength (UTS) after HPT is ~1.75 GPa and the elongation to failure is only ~4% and this compares with a strength and elongation to failure in the initial homogenized condition of ~440 MPa and 85%, respectively.

Figure 9 reveals also that PDA at 773 and 873 K leads to a drop in strength and the elongation to failure remains very low to the extent that the elongation to failure after annealing at 873 K is lower than immediately after HPT processing. Thus, the stress-strain curves of the samples after PDA at these temperatures show the typical mechanical properties of brittle materials and this behaviour is attributed to the formation of precipitates in the microstructure during PDA. According to the high volume fractions of precipitates during PDA at temperatures below 773 K, it is reasonable to anticipate a brittle behaviour during tensile testing. Annealing at 973 K gives a reasonably high flow stress that is a direct consequence of the HPT processing but there is also an improvement in the elongation to failure compared with the HPT sample or the samples subjected to PDA at lower temperatures. The elongations to failure of samples subjected to PDA at 1073 or 1173 K show a significant improvement in the elongation to failure by comparison with the samples annealed at lower temperatures but with a corresponding reduction in the UTS. Table 2 summarizes all of the mechanical properties data derived from the samples shown in Fig. 9.

Thus, PDA at temperatures of 1073 and 1173 K appears to be the optimum condition for attaining reasonable strength coupled with a high ductility. Accordingly, the HPT-processed samples were subjected to short-term PDA at these temperatures for different times and the representative plots of engineering stress against engineering strain using an initial strain rate of 1.0×10^{-3} s^{-1} are shown in Fig. 10 and the mechanical properties are summarized in Table 2

after HPT followed by PDA at 1073 and 1173 K for times of 10, 30 and 60 min. It appears from these data that the strength decreases consistently with increasing annealing time but there is no significant change in the elongations to failure after PDA for 30 min. According to these results, PDA at 1073 K for 10 min leads to very good mechanical properties with a UTS of ~830 MPa and an elongation to failure of ~65%.

4. Discussion

4.1 *Microstructural evolution during HPT processing and mechanical properties*

These microstructural observations reveal exceptional grain refinement to ~10 nm and the formation of a single-phase nanocrystalline CoCrFeNiMn HEA after HPT processing. In this condition, the grain interiors contain many twin boundaries as shown in Fig. 3(b).

Thus, one of the main features of the microstructural evolution of the high entropy CoCrFeNiMn alloy during HPT processing is intensive deformation twinning and these twin boundaries may have a significant influence on the evolution and/or the refinement of the microstructure during further straining following the saturation of twinning [28-31]. In fact, the introduction of extra interfaces within the grains during deformation twinning leads to significant grain refinement and extraordinary increments in hardness and UTS after HPT processing at room temperature [32]. It is expected that the formation of twins will lead to continuous grain subdivision through the introduction of new interfaces which effectively reduce the dislocation mean free path and cause hardening. Another hardening mechanism is substructure hardening due to the dislocation density [30]. The very high ductility of the alloy in the homogenized condition is most likely associated with the intensive twinning [31] and therefore the decrease in ductility in the HPT-processed samples is a consequence of the cessation of twining at large strains.

These mechanical results clearly show significant hardening after HPT processing of the CoCrFeNiMn HEA. The microhardness and the UTS indicate increments of 270% and 290%, respectively, after HPT processing through 5 turns.

4.2 *Microstructural evolution during post-deformation annealing*

The initial and HPT-processed microstructures consist of a single *fcc* phase. However, the substantial increase in hardness upon annealing, combined with XRD and microstructural evaluations, suggest that phase decomposition takes place during PDA at 473-973 K. The decomposition and formation of new phases in the *fcc*-matrix phase was reported earlier in different HEAs after annealing within special temperature ranges [19,20,24,33-36]. It was suggested that Cr promotes the formation of a *bcc* phase and, based on thermodynamic calculations, solubility of Cr in the *fcc* phase is quite high at high temperatures but decreases with decreasing temperature giving rise to the formation of a Cr-rich *bcc* phase. It was shown that the CoCrFeMnNi alloy has a single-phase *fcc* structure above 873 K while a mixture of *fcc* and *bcc* phases, or under some conditions an σ phase with a tetragonal crystal structure, forms below 873 K [19,24]. The present results confirm the formation of a multi-phase nanostructured HEA after PDA up to 973 K consisting of a Cr-rich *bcc* phase homogenously distributed in the microstructure and nano-scale precipitates homogenously distributed in the primary *fcc* phase. According to the TEM results in Figs 6(d) and 7, the latter precipitates are a σ Cr-rich phase and MnNi-rich phases.

The nano-scale precipitates, consisting of a MnNi phase and a Cr-rich phases, were reported after HPT processing of the alloy followed by short-term annealing at 723 K and Cr- and Mn-rich grain boundary precipitates were observed after low strain rate creep at 1073 K [37]. In addition, grain boundary precipitates enriched in Cr, containing some Mn, Fe and Co but very little Ni (σ-phase), were reported recently after very long-term annealing of a coarse-grained CoCrFeNiMn HEA at 973 K [19,20]. It is important to note that, unlike the HPT condition, the

σ phase was not detected in the present sample after annealing the homogenized condition prior to HPT. It appears that the nanocrystalline grain structure of the HPT processed HEA facilitates the phase decomposition owing to the large number of grain boundaries which serve both as fast diffusion pathways and also as preferential nucleation sites for the formation of new phases. A recent report demonstrated the occurrence of fast diffusion in a nanocrystalline HEA due to the presence of severe torsion stresses [13]. Thus, in the present study the heavy deformation leads more quickly to the formation of stable phases than in the absence of any mechanical treatment.

The results indicate that recrystallization occurs after PDA at T>973 K and this is consistent with the dissolution of the precipitates. Generally, the HEA has a high recrystallization temperature and a strong resistance against grain coarsening during annealing [38-41]. Close inspection of the hardness results shows the hardness decreases significantly above 773 K due to dissolution of the precipitates and activation of the recrystallization mechanism up to 1173 K so that finally the hardness is equal to the homogenized condition due to grain growth. A systematic study of grain growth in an *fcc* single-phase CoCrFeNiMn HEA after heavy plastic deformation suggested that the grains coarsen at a temperature above 1123 K and grain boundary motion is then controlled by a solute-drag mechanism [39]. At a significantly high recrystallization temperature (>973 K), low grain growth rate and the ultrafine-grained structure of the HEA is attributed to the distorted matrix which is characterized by a high lattice distortion energy, a sluggish diffusion effect and a low stacking fault energy [40]. The stability of hardness after increasing the annealing time at each temperature, as shown in Fig. 4(b), confirms the effect of sluggish diffusion in the alloy. The as-recrystallized samples and samples experiencing grain growth show twins.

4.3 Mechanical properties after post-deformation annealing

Despite the success in achieving a highly-refined microstructure, it is readily apparent from

Fig. 9 that the tensile properties of the HPT-processed specimens are not satisfactory when testing at room temperature. Accordingly, PDA of nanostructured CoCrFeNiMn HEA is necessary for improving the ductility. However, the results show the formation of precipitates after PDA at 473-973 K so that the material is brittle. It appears that the newly-formed phases have an intermetallic character which is generally considered to provide high strength [12]. The strength at these conditions can be envisaged by considering the microstructure as a nano-composite consisting of several phases differing markedly in their intrinsic strength.

Based on energetic considerations, the nucleation sites for the new phases are assumed to lie on the grain boundaries of the matrix phase. The precipitation of second phases at grain boundaries may hinder dislocation emission and motion at grain boundaries. However, it is apparent from Figs 6 and 7 that annealing at low temperatures after HPT processing leads to the formation of a Cr-rich *bcc* phase having typical dimensions similar to those of the primary phase which are several tens of nanometers after PDA at 873 K and 400 nm after PDA at 873 K. Therefore, the strengthening is not exclusively explained by precipitation at the grain boundaries. For classical precipitation hardening, the precipitates are situated within the individual grains and remain small compared to the grain size so that they are effective obstacles for dislocation motion as in dispersion hardening [42]. The nano-scale precipitates formed in the matrix grains of the present alloy are consistent with this behavior.

According to the formation of precipitates which cause brittleness in the HEA, especially at 873 and 973 K where the σ phase is stable, it appears that PDA at T>973 K maintains the strength at a reasonable level while the ductility is regained. It is important to note that the volume fraction of the precipitated phases is negligible at 1073 K but the results indicate grain coarsening at a temperature above 1073 K. It was suggested that the alloy softens as the grains grow above 1023 K and the strength of the alloy obeys the classical Hall-Petch relationship although the hardening coefficient is larger than obtained in conventional *fcc* metals [39].

Due to the significantly destructive effect of brittle precipitates, especially the σ phase, on ductility in the HPT-processed HEA and the reduction in the effect of annealing at excessively high temperatures due to recrystallization, selecting an appropriate annealing condition may produce both good ductility and high strength in the nanostructured HEA. Therefore, short-term PDA at 1073 and 1173 K offers the best approach for preventing grain growth and obtaining a combination of high strength and good ductility in the HPT-processed HEA. It is important to note also that sluggish diffusion in the HEA is helpful in achieving this objective. It is well established that short-term annealing after HPT processing is an effective and simple procedure for achieving good strength and reasonable levels of ductility [43-45].

The elongation to failure of samples after PDA at 1073 and 1173 K shows a significant improvement by comparison with other PDA conditions and even with the homogenized sample. Inspection of Tables 1 and 2 reveals that PDA at a temperature of 1073 K is the optimum condition for attaining reasonable strength coupled with a high ductility. Thus, PDA at 1073 K for 10 min leads to good mechanical properties with a UTS and elongation to failure of ~830 MPa and ~65%, respectively.

5. Summery and conclusions

1. A CoCrFeNiMn high-entropy alloy was processed by HPT under 6.0 GPa pressure up to 10 turns at room temperature. Following processing, the average grain size was reduced to ~10 nm and this was accompanied by an exceptional increase in the hardness and UTS.

2. The hardness of the HEA further increased after PDA at temperatures up to 773 K due to the formation of new precipitates. The hardness decreased after annealing at higher temperatures up to 1173 K due to recrystallization and precipitate dissolution.

3. The formation of a brittle σ phase at 873 and 973 K showed that PDA at temperatures above 973 K was the optimum condition for maintaining strength at a reasonable level and attaining good ductility but PDA above 1073 K led to grain growth and a consequent decrease

in strength. Short-term annealing at 1073 and 1173 K is the best procedure for preventing grain growth and obtaining a combination of high strength and good ductility. Specifically, PDA at 1073 K for 10 min leads to good mechanical properties with a UTS and elongation to failure of ~830 MPa and ~65%, respectively.

Acknowledgments

JYH and ZPL acknowledge financial support from the National Natural Science Foundation of China (No. 51531001). MK was supported in part by the NRF Korea funded by MoE under Grant No. NRF-2014R1A1A2057697 and NRF-2016R1A6A1A03013422. This work was supported by the European Research Council under Grant Agreement No. 267464-SPDMETALS.

References

1. J.W. Yeh, S.K. Chen, S.J. Lin, J.Y. Gan, T.S. Chin, T.T. Shun, C.H. Tsau, S.Y. Chang, Nanostructured high-entropy alloys with multiple principal elements: novel alloy design concepts and outcomes, Adv. Eng. Mater. 6 (2004) 299-303.

2. B. Cantor, I.T.H. Chang, P. Knight, A.J.B. Vincent, Microstructural development in equiatomic multicomponent alloys, Mater. Sci. Eng. A 375-377 (2004) 213-218.

3. F. Otto, A. Dlouhý, Ch. Somsen, H. Bei, G. Eggeler, E.P. George, The influences of temperature and microstructure on the tensile properties of a CoCrFeMnNi high-entropy alloy, Acta Mater. 61 (2013) 5743-5755.

4. F. Otto, Y. Yang, H. Bei, E.P. George, Relative effects of enthalpy and entropy on the phase stability of equiatomic high-entropy alloys, Acta Mater. 61 (2013) 2628-2638.

5. B. Gludovatz, A. Hohenwarter, D. Catoor, E.H. Chang, E.P. George, R.O. Ritchie, A fracture-resistant high-entropy alloy for cryogenic applications, Science 345 (2014) 1153-1158.

6. A.P. Zhilyaev, T.G. Langdon, Using high-pressure torsion for metal processing: Fundamentals and applications, Prog. Mater. Sci. 53 (2008) 893-979.

7. R. Valiev, Nanomaterial advantage, Nature 419 (2002) 887-889.

8. C.C. Koch, Optimization of strength and ductility in nanocrystalline and ultrafine grained metals, Scr. Mater. 49 (2003) 657-662.

9. R. Valiev, Nanostructuring of metals by severe plastic deformation for advanced properties, Nat. Mater. 3 (2004) 511-516.

10. R.Z. Valiev, A.V. Sergueeva, A.K. Mukherjee, The effect of annealing on tensile deformation behaviour of nanostructured SPD titanium, Scr. Mater. 49 (2003) 669-674.

11. Q.H. Tang, Y. Huang, Y.Y. Huang, X.Z. Liao, T.G. Langdon, P.Q. Dai, Hardening of an $Al_{0.3}$CoCrFeNi high entropy alloy via high-pressure torsion and thermal annealing, Mater. Lett. 151 (2015) 126-129.

12. B. Schuh, F. Mendez-Martin, B. Völker, E.P. George, H. Clemens, R. Pippan, A. Hohenwarter, Mechanical properties, microstructure and thermal stability of a nanocrystalline CoCrFeMnNi high-entropy alloy after severe plastic deformation, Acta Mater. 96 (2015) 258-268.

13. D-H. Lee, I-C. Choi, M-Y. Seok, J. He, Z. Lu, J-Y. Suh, M. Kawasaki, T.G. Langdon, J-I. Jang, Nanomechanical behavior and structural stability of a nanocrystalline CoCrFeNiMn high-entropy alloy processed by high-pressure torsion, J. Mater. Res. 30 (2015) 2804-2815.

14. P.F. Yu, H. Cheng, L.J. Zhang, H. Zhang, Q. Jing, M.Z. Ma, P.K. Liaw, G. Li, R.P. Liu, Effects of high pressure torsion on microstructures and properties of an $Al_{0.1}$CoCrFeNi high-entropy alloy, Mater. Sci. Eng. A 655 (2016) 283-291.

15. Q.H. Tang, Y. Huang, H. Cheng, X.Z. Liao, T.G. Langdon, P.Q. Dai, The effect of grain size on the annealing-induced phase transformation in an $Al_{0.3}$CoCrFeNi high entropy alloy, Mater. Design 105 (2016) 381-385.

16. D-H. Lee, M-Y. Seok, Y. Zhao, I-C. Choi, J. He, Z. Lu, J-Y. Suh, U. Ramamurty, M. Kawasaki, T.G. Langdon, J-I. Jang, Spherical nanoindentation creep behavior of nanocrystalline and coarse-grained CoCrFeMnNi high-entropy alloys, Acta Mater. 109 (2016) 314-322.

17. R.B. Figueiredo, P.R. Cetlin, T.G. Langdon, Using finite element modelling to examine the flow processes in quasi-constrained high-pressure torsion, Mater. Sci. Eng. A 528 (2011) 8198-8204.

18. F. Otto, N.L. Hanold, E.P. George, Microstructural evolution after thermomechanical processing in an equiatomic, single-phase CoCrFeMnNi high-entropy alloy with special focus on twin boundaries, Intermetallics 54 (2014) 39-48.

19. F. Otto, A. Dlouhý, K.G. Pradeep, M. Kuběnová, D. Raabe, G. Eggeler, E.P. George, Decomposition of the single-phase high-entropy alloy CrMnFeCoNi after prolonged anneals at intermediate temperatures, Acta Mater. 112 (2016) 40-52.

20. E.J. Pickering, R. Muñoz-Moreno, H.J. Stone, N.G. Jones, Precipitation in the equiatomic high-entropy alloy CrMnFeCoNi, Scr. Mater. 113 (2016) 106-109.

21. J. Wang J, Z. Horita, M. Furukawa, M. Nemoto, N.K. Tsenev, R.Z. Valiev, Y. Ma, T.G. Langdon, An investigation of ductility and microstructural evolution in an Al-3% Mg alloy with submicron grain size, J. Mater. Res. 8 (1993) 2810-2818.

22. Z. Zhang, F. Zhou, E. J. Lavernia, On the analysis of grain size in bulk nanocrystalline materials via X-ray, Metall Mater Trans. A, 34A (2003) 1349-1355.

23. M.H. Tsai, H. Yuan, G. Cheng, W. Xu, W.W. Jian, M.H. Chuang, C.C. Juan, A.C. Yeh, S.J. Lin, Y. Zhu, Significant hardening due to the formation of a sigma phase matrix in a high entropy alloy, Intermetallics 33 (2013) 81-86.

24. F. Zhang, C. Zhang, S.L. Chen, J. Zhu, W.S. Cao, U.R. Kattner, An understanding of high entropy alloys from phase diagram calculations, CALPHAD 45(2014)1-10.

25. R.Z. Valiev, V.Yu. Gertsman, O.A. Kaibyshev, Grain boundary structure and properties under external influences, Phys. Stat. Sol. (a) 97 (11) (1986) 11-56.

26. R.Z. Valiev, I.V. Alexandrov, Y.T. Zhu, T.C. Lowe, Paradox of strength and ductility in metals processed by severe plastic deformation, J. Mater. Res. 17 (2002) 5-8.

27. P. Kumar, M. Kawasaki, T.G. Langdon, Review: Overcoming the paradox of strength and ductility in ultrafine-grained materials at low temperatures, J. Mater. Sci. 51 (2016) 7-18.

28. J.W. Christian, S. Mahajan, Deformation twinning, Prog. Mater. Sci. 39 (1995) 1-157.

29. G. Salishchev, S. Mironov, S. Zherebtsov, A. Belyakov, Changes in misorientations of grain boundaries in titanium during deformation, Mater. Charact. 61 (2010) 732-739.

30. S.V. Zherebtsov, G.S. Dyakonov, A.A. Salem, V.I. Sokolenko, G.A Salishchev, S.L. Semiatin, Formation of nanostructures in commercial-purity titanium via cryo-rolling, Acta Mater. 61 (2013) 1167-1178.

31. N. Stepanov, M. Tikhonovsky, N. Yurchenko, D. Zyabkin, M. Klimova, S. Zherebtsov, A. Efimov, G. Salishchev, Effect of cryo-deformation on structure and properties of CoCrFeNiMn high-entropy alloy, Intermetallics 59 (2015) 8-17.

32. K. Lu, L. Lu, S. Suresh, Strengthening materials by engineering coherent internal boundaries at the nanoscale, Science 324 (2009) 349-352.

33. C.W. Tsai, Y.L. Chen, M.H. Tsai, J.W. Yeh, T.T. Shun, S.K. Chen, Deformation and annealing behaviors of high-entropy alloy Al0.5CoCrCuFeNi, J. Alloys Compd. 486 (2009) 427-435.

34. C. Ng, S. Guo, J. Luan, S. Shi, C.T. Liu, Entropy-driven phase stability and slow diffusion kinetics in an Al0.5CoCrCuFeNi high entropy alloy, Intermetallics 31 (2012) 165-172.

35. M. Laurent-Brocq, A. Akhatova, L. Perrière, S. Chebini, X. Sauvage, E. Leroy, Y. Champion, Insights into the phase diagram of the CrMnFeCoNi high entropy alloy, Acta Mater. 88 (2015) 355-365.

36. J.Y. He, H. Wang, H.L. Huang, X.D. Xu, M.W. Chen, Y. Wu, X.J. Liu, T.G. Nieh, K. An, Z.P. Lu, A precipitation-hardened high-entropy alloy with outstanding tensile properties, Acta Mater. 102 (2016) 187-196.

37. J.Y. He, C. Zhu, D.Q. Zhou, W.H. Liu, T.G. Nieh, Z.P. Lu, Steady state flow of the FeCoNiCrMn high entropy alloy at elevated temperatures, Intermetallics 55 (2014) 9-14.

38. K.Y. Tsai, M.H. Tsai, J.W. Yeh, Sluggish diffusion in Co–Cr–Fe–Mn–Ni high-entropy alloys, Acta Mater. 61 (2013) 4887-4897.

39. W.H. Liu, Y. Wu, J.Y. He, T.G. Nieh, Z.P. Lu, Grain growth and the Hall-Petch relationship in a high-entropy FeCrNiCoMn alloy, Scr Mater 68 (2013) 526-529.

40. P.P. Bhattacharjee, G.D. Sathiaraj, M. Zaid, J.R. Gatti, Chi Lee, Che-Wei Tsai, Jien-Wei Yeh, Microstructure and texture evolution during annealing of equiatomic CoCrFeMnNi high-entropy alloy, J. Alloy. Compd. 587 (2014) 544-552.

41. G. Dan Sathiaraj, P.P. Bhattacharjee, Analysis of microstructure and microtexture during grain growth in low stacking fault energy equiatomic CoCrFeMnNi high entropy and Ni-60 wt.%Co alloys, J. Alloy. Compd. 637 (2015) 267-276.

42. R.F. Decker, Alloy design using second phases, Metall. Trans. 4 (1973) 2495-2518.

43. O. Andreau, J. Gubicza, N.X. Zhang, Y. Huang, P. Jenei, T.G. Langdon, Effect of short-term annealing on the microstructures and flow properties of an Al-1% Mg alloy processed by high-pressure torsion, Mater. Sci. Eng. A 615 (2014) 231-239.

44. N. Maury, N.X. Zhang, Y. Huang, A.P. Zhilyaev, T.G. Langdon, A critical examination of pure tantalum processed by high-pressure torsion, Mater. Sci. Eng. A 638(2015)174-182.

45. Y. Huang, M. Lemang, N.X. Zhang, P.H.R. Pereira, T.G. Langdon, Achieving superior grain refinement and mechanical properties in vanadium through high-pressure torsion and subsequent short-term annealing, Mater. Sci. Eng. A 655 (2016) 60-69.

Table 1. Volume fraction of precipitates, grain size (d), microhardness, YS, UTS and elongation (δ) of CoCrFeNiMn HEA before and after PDA at 473 to 1173 K for 60 min.

Annealing temperature (K)	Precipitates (%)	d	Hv	YS (MPa)	UTS (MPa)	δ (%)
HPT	0	~10 nm[a,b]	450	1400	1740	4
473	~19	~15 nm[a]	490	-	-	-
673	~20	~30 nm[a]	515	-	-	-
773	~17	~60 nm[a]	520	930	1250	5
873	~10	~90 nm[b]	455	1010	1060	2
973	~7	~400 nm[b]	355	950	1030	21
1073	~5	~4 μm[b]	220	530	680	80
1173	0	~17 μm[b]	140	370	600	90

[a] Based on XRD results.

[b] Based on microscopic observations.

Table 2. Microhardness, YS, UTS and elongation (δ) of CoCrFeNiMn HEA before HPT and after PDA at 1073 to 1173 K for 10 to 60 min.

Annealing temperature (K)	Annealing time (min)	Hv	YS (MPa)	UTS (MPa)	δ (%)
Homogenized	-	120	300	530	85
1073	10	290	680	830	65
	30	245	570	725	78
	60	220	530	680	80
1173	10	170	410	630	76
	30	155	390	610	80
	60	140	370	600	90

Fig. 1 (a) Values of the Vickers microhardness measured across disks processed from 1 to 10 turns at a rotation speed of 1 rpm: the lower dashed line shows the homogenized initial condition. (b) Values of the Vickers microhardness plotted against the equivalent strain after processing by HPT through various numbers of turns.

Fig. 2. X-ray patterns of the homogenized (N = 0) condition and near the edge of the disks processed from 1 to 5 turns at a rotation speed of 1 rpm.

Fig. 3. (a) Optical micrograph of the microstructure of the CoCrFeNiMn alloy after homogenizing: white arrows show Cr-Mn oxides. (b) TEM image and corresponding SAED pattern after 5 turns HPT processing: arrows show nano-twins in nano-grains.

Fig. 4. (a) Dependence of Vickers hardness of the homogenized and HPT-processed samples on the annealing temperature; the annealing time is 60 min. (b) Dependence of Vickers hardness of the HEA after HPT on the annealing time at different annealing temperatures.

Fig. 5. X-ray patterns near the edges of disks after HPT processing followed by PDA at 473 to 1173 K for 60 min.

Fig. 6. TEM images and corresponding SAED patterns after 5 turns of HPT processing followed by PDA at 873 K for 60 min: (a) Equiaxed grains in the range of ~40-120 nm with a mean grain size of ~90 nm, (b) chemical analyses of two neighbouring grains reported in at.% after EDS analysis: nano precipitates and twins are shown by arrows in the microstructure, (c) EDS chemical analysis and corresponding SAED pattern of a grain containing nano precipitates, (d) nano precipitates, contours and twins shown by arrows in the microstructure.

Fig. 7. SAED patterns after 5 turns of HPT processing (left) and PDA at 873 K for 60 min (right).

Fig. 8. (a) SEM observation after PDA at 973 K; arrow shows precipitated phase in the matrix. (b-d) OM observation after PDA at 973 to 1173 K; arrow shows ultra-fine grains in (b).

Fig. 9. Stress-strain curves at an initial strain rate of 1.0×10^{-3} s^{-1} in the homogenized and HPT-processed conditions and after PDA at 773 to 1173 K for 60 min.

Fig. 10. Stress-strain curves at an initial strain rate of 1.0×10^{-3} s^{-1} after PDA at (a) 1073 and (b) 1173 K for 10-60 min.

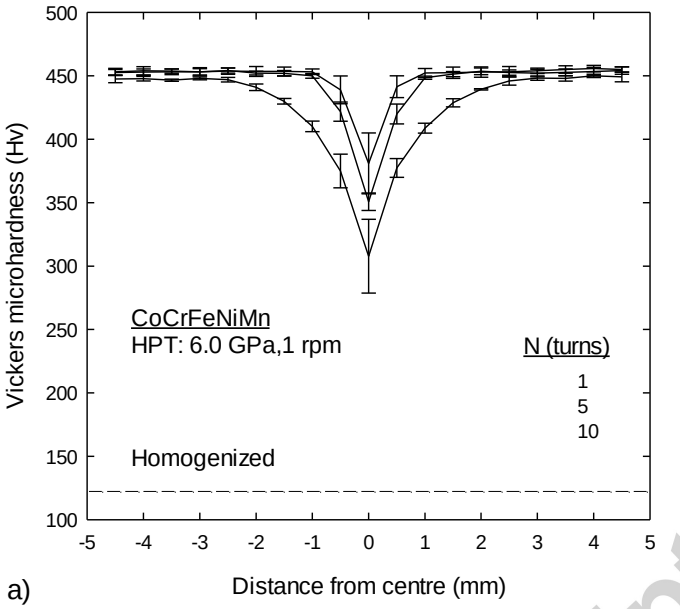

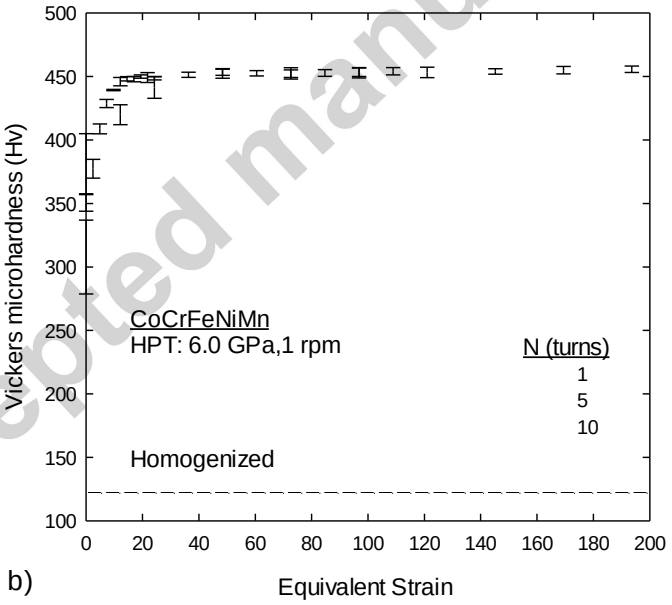

Fig. 1 (a) Values of the Vickers microhardness measured across disks processed from 1 to 10 turns at a rotation speed of 1 rpm: the lower dashed line shows the homogenized initial condition. (b) Values of the Vickers microhardness plotted against the equivalent strain after processing by HPT through various numbers of turns.

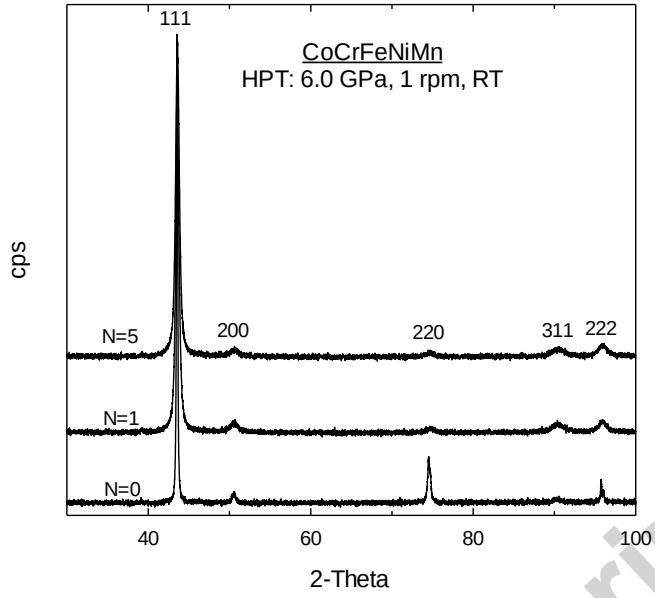

Fig. 2. X-ray patterns of the homogenized (N = 0) condition and near the edge of the disks processed from 1 to 5 turns at a rotation speed of 1 rpm.

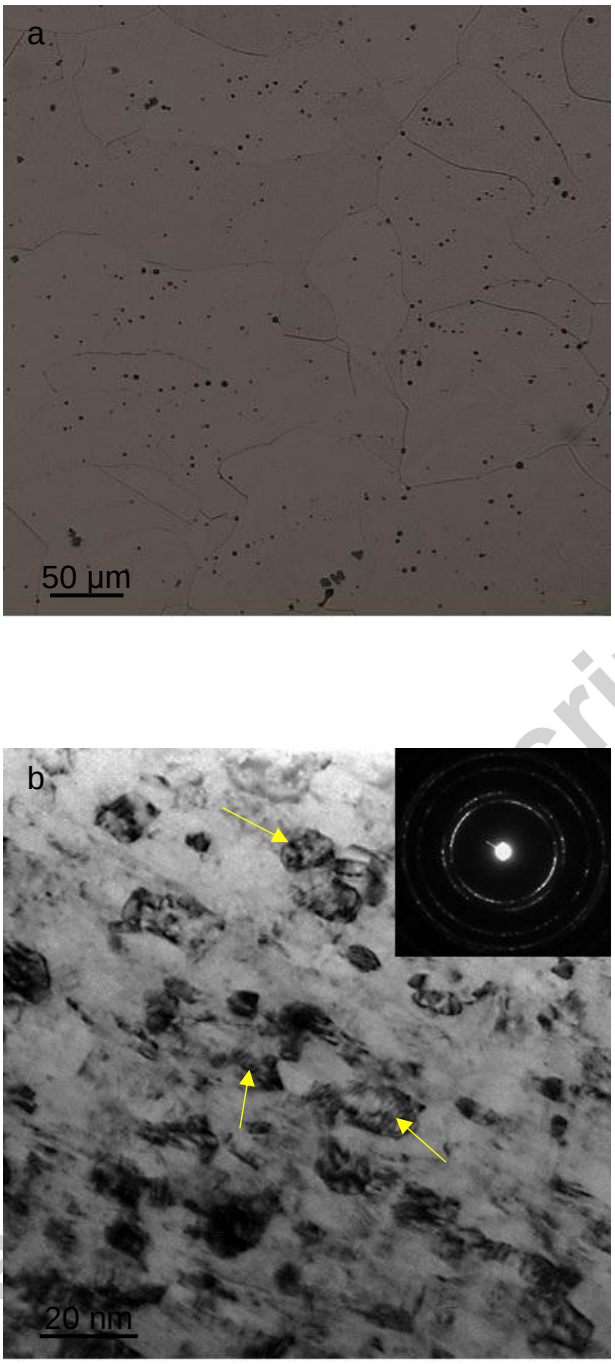

Fig. 3. (a) Optical micrograph of the microstructure of the CoCrFeNiMn alloy after homogenizing: white arrows show Cr-Mn oxides. (b) TEM image and corresponding SAED pattern after 5 turns HPT processing: arrows show nano-twins in nano-grains.

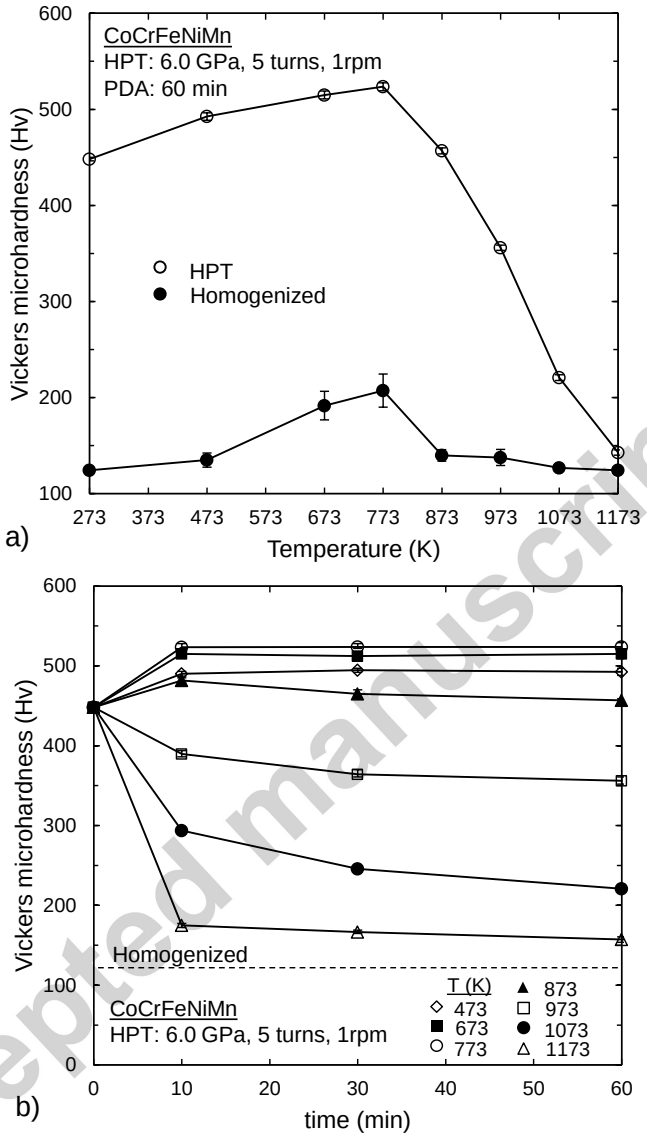

Fig. 4. (a) Dependence of Vickers hardness of the homogenized and HPT-processed samples on the annealing temperature; the annealing time is 60 min. (b) Dependence of Vickers hardness of the HEA after HPT on the annealing time at different annealing temperatures.

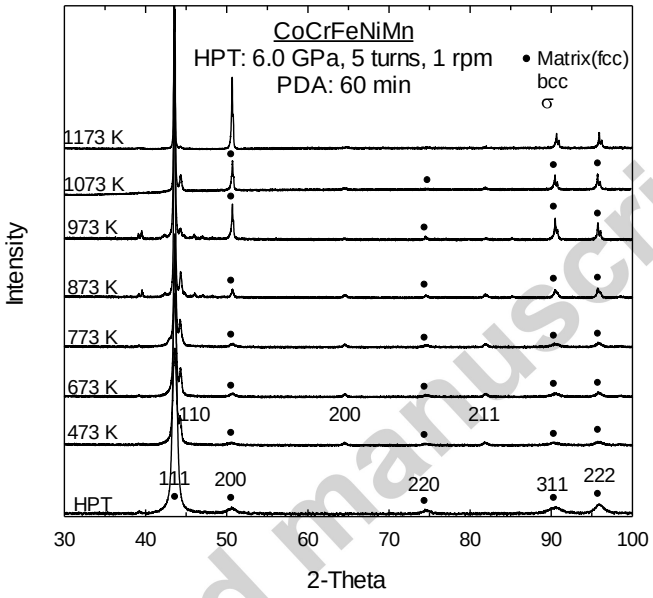

Fig. 5. X-ray patterns near the edge of disks after HPT processing followed by PDA at 473 to 1173 K for 60 min.

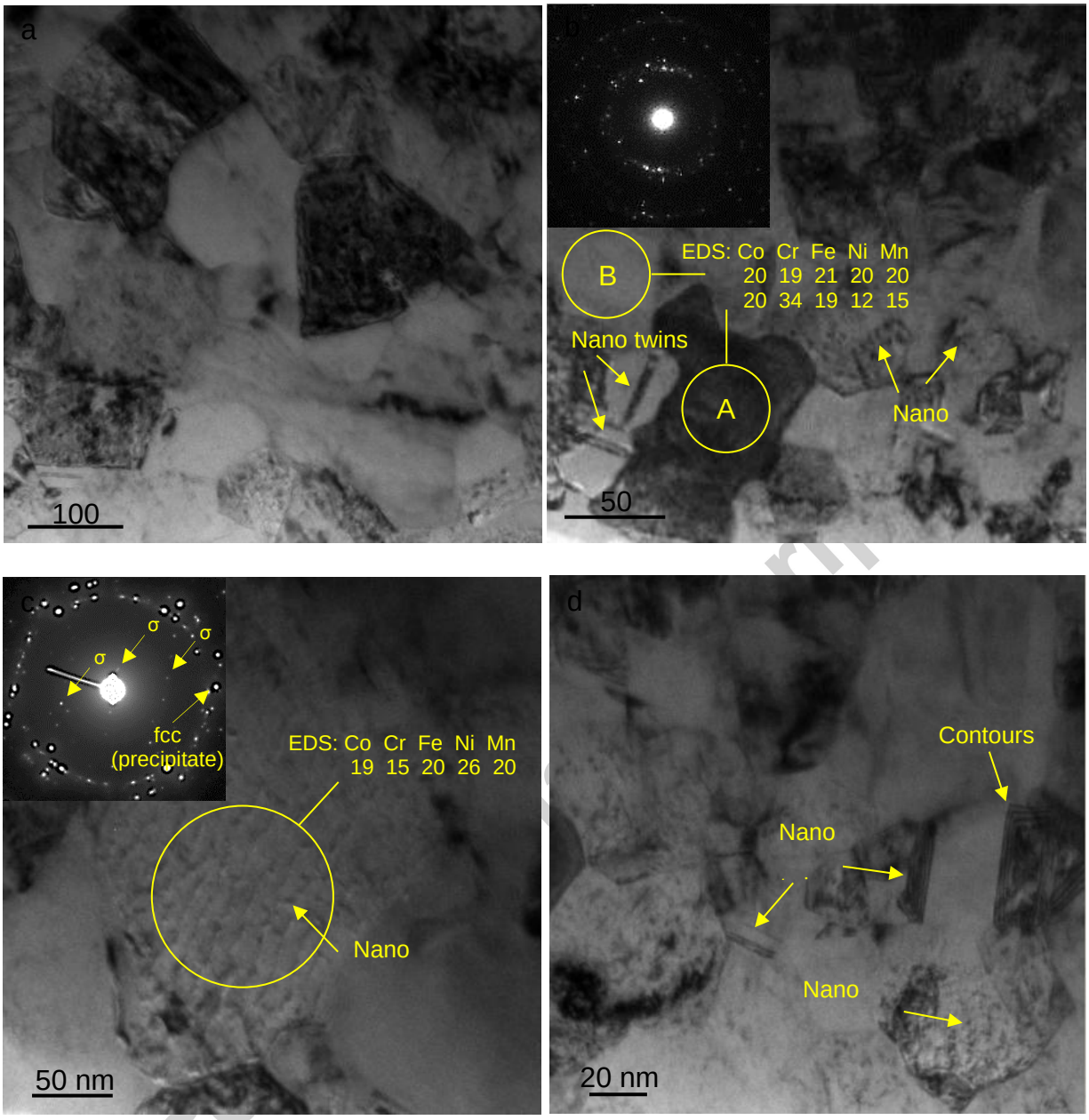

Fig. 6. TEM images and corresponding SAED patterns after 5 turns HPT processing followed by PDA at 873 K for 60 min; (a) Equiaxed grains in the range of ~40-120 nm with the mean grain size of ~90 nm, (b) chemical analyses of two neighbouring grains are reported in at.% after EDS analysis: nano precipitates and annealing twins are shown by arrows in the microstructure, (c) EDS chemical analyse and corresponding SAED pattern of a grain which contains nano precipitates, (d) nano precipitates, contours and twins are shown by arrows in the microstructure.

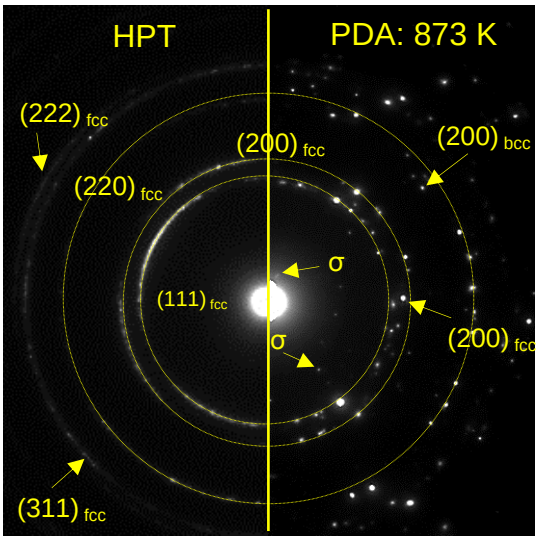

Fig. 7. SAED patterns after 5 turns HPT processing (left) and PDA at 873 K for 60 min (right).

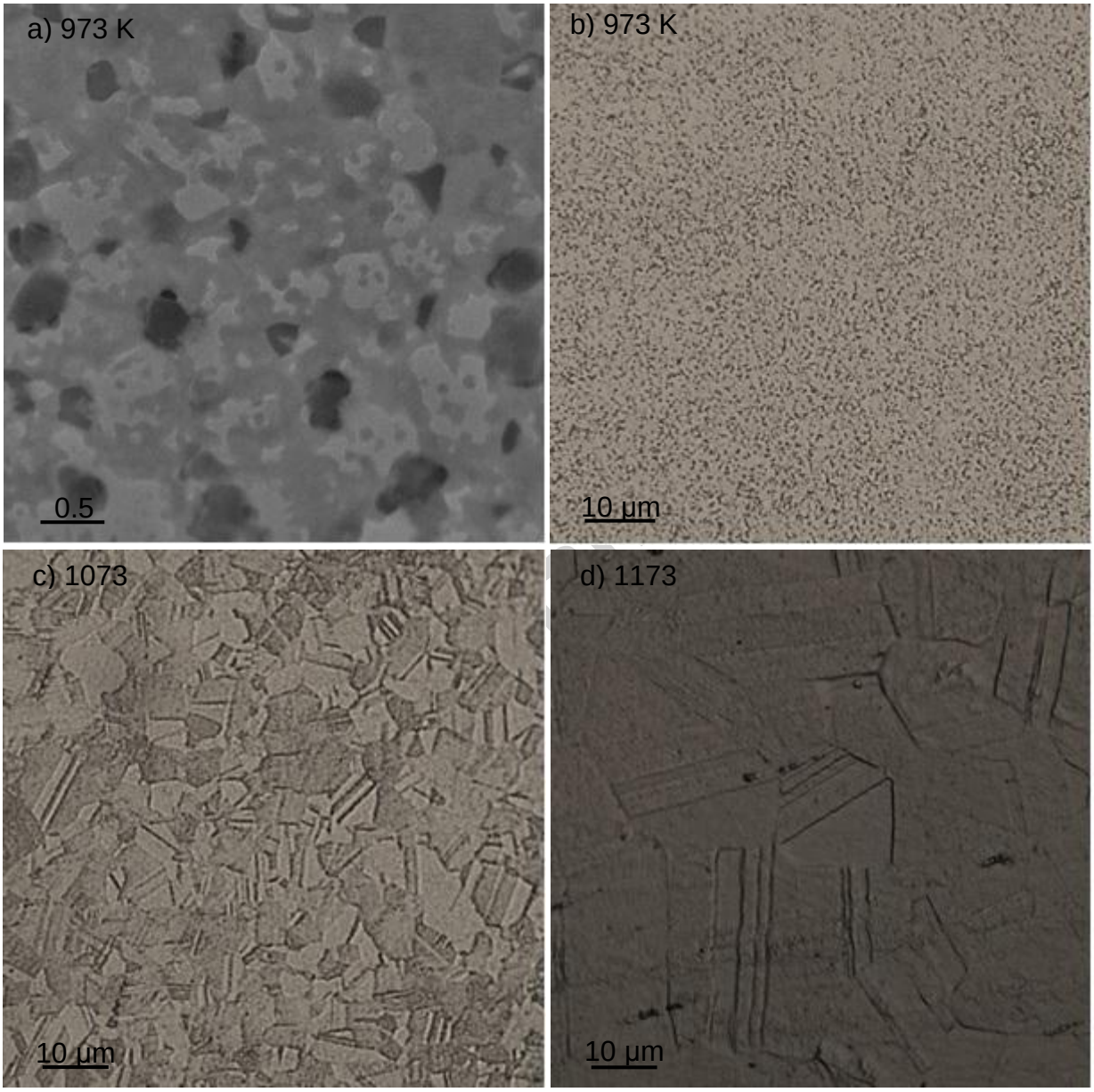

Fig. 8. (a) SEM observation after PDA at 973 K; arrow shows precipitated phase in the matrix.

(b-d) OM observation after PDA at 973 to 1173 K; arrow shows ultra-fine grains in (b).

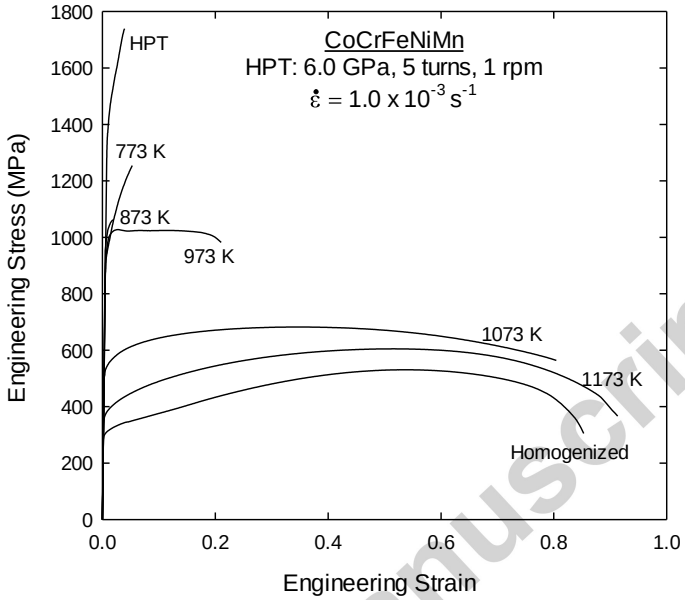

Fig. 9. Stress-strain curves at an initial strain rate of 1.0×10^{-3} s^{-1} in the homogenized and HPT-processed conditions and PDA at 773 to 1173 K for 60 min.

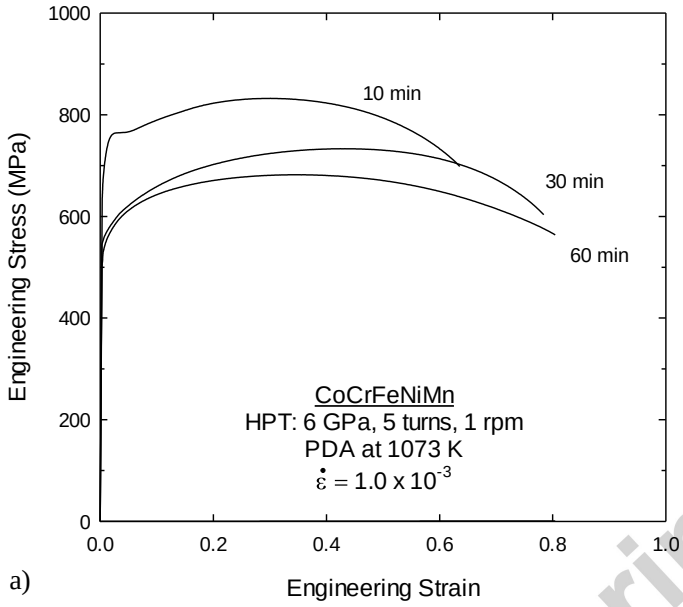

a)

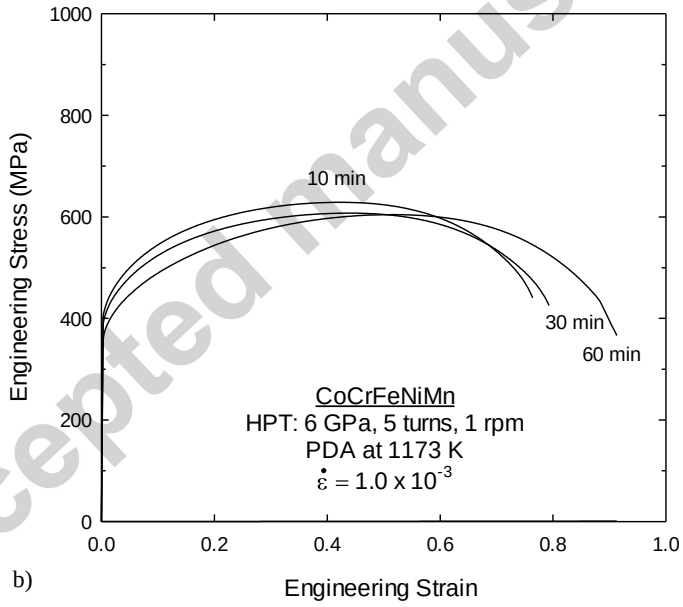

b)

Fig. 10. Stress-strain curves at an initial strain rate of 1.0×10^{-3} s^{-1} after PDA at (a) 1073 and (b) 1173 K for 10-60 min.